IET Renewable Power Generation

Special Issue Call for Papers

Be Seen. Be Cited.
Submit your work to a new IET special issue

Connect with researchers and experts in your field and share knowledge.

Be part of the latest research trends, faster.

Read more

The Institution of Engineering and Technology

IET Renewable Power Generation

Special Issue: Selected papers from the 7th International Conference on Clean Electrical Power (ICCEP 2019)

IET Journals
The Institution of Engineering and Technology

Experimental assessment of winding inter-turn short-circuits fault signatures in six-phase AC permanent magnet synchronous motors

ISSN 1752-1416
Received on 2nd February 2020
Revised 18th March 2020
Accepted on 8th April 2020
E-First on 5th November 2020
doi: 10.1049/iet-rpg.2020.0055
www.ietdl.org

Yasser Gritli[1,2] ✉, Michele Mengoni[1], Claudio Rossi[1], Angelo Tani[1], Domenico Casadei[1], Giovanni Serra[1]

[1]DEI – Department of Electrical, Electronic and Information Engineering - Guglielmo Marconi, University of Bologna, Bologna 40126, Italy

[2]Department of Electrical Engineering, LARA-ENIT (LR-11-ES18), National Engineering School of Tunis University of Tunis El Manar, Tunis, Belvedere 1002, Tunisia

✉ *E-mail: yasser.gritli@unibo.it*

Abstract: The interest for multiphase permanent magnet synchronous machines, in modern renewable power generation systems, is increasing rapidly due principally to their high efficiency and fault-tolerant capability. To meet the high-performance requirements, monitoring the stator winding state is a key item. The detectability of a stator winding inter-turn short-circuit (ITSC), for an asymmetrical six-phase surface-mounted permanent magnet synchronous motor, is analysed in this study. The impact of an ITSC on the stator back-emfs, stator currents and voltages is examined by spectral analysis of the corresponding space-vectors, in different α–β planes. In particular, the detectability of a stator ITSC, in closed-loop operating conditions, is investigated using voltage and current signature analysis. The spectral fault signature is identified through 2D finite element analysis, and then confirmed by laboratory experimental tests.

1 Introduction

Multiphase machines are receiving increasing interest in the field of modern renewable power generation systems (RPGSs), and especially for wind energy conversion systems (WECSs). Combining the typical properties of high-power density as well as the typical high torque-to-inertia ratio of permanent magnet synchronous machines (PMSMs) with the features of multiphase machines topology leads to higher reliability and efficiency.

Nowadays, multiphase PMSMs (m-PMSMs) are well established as an attractive alternative to classical 3-PMSMs for achieving high power ratings without growing the current/phase, leading to a derating of the power switches of the required inverter for feeding the machine. Moreover, with reference to traditional 3-PMSM drives, m-PMSM drives exhibit crucial benefits providing higher torque ripple frequency with reduced amplitude, and greater degrees of freedom, allowing higher fault-tolerant capabilities [1–3].

Multiple three-phase winding sets are the most common configuration of m-PMSM, since each three-phase winding set can be individually supplied by a conventional three-phase inverter, which is a mature technology and widely available at a reasonable cost. This category of m-PMSMs allows splitting the total rated power between the different winding sets, thus enhancing the efficiency of the whole drive with lower losses [4, 5]. So, it is straightforward that the above-mentioned m-PMSM characteristics are particularly advantageous in terms of design and maintainability for modern multi-megawatt full-power WECSs. Although the advantages of m-PMSMs, they are still subjected to stator winding faults. As mentioned in [6], it was stated that stator windings faults account for 40% of the overall electric machine failures in petroleum and chemical industries. Due to more windings on the stator side, m-PMSMs are more prone to stator failures than classical 3-PMSMs.

There are different forms of stator failures that can affect m-PMSMs, leading to degraded performances of the machine, such as inter-turn short-circuit (ITSC), line-to-line, line-to-ground, multi-phase line-to-ground, or multi-phase mixed faults. A detailed analysis of these kinds of faults and its propagation and diagnosis can be found in [1–3].

Specifically, the ITSC is well known as one of the most difficult and complex stator failures to detect. Due to the combination of electromechanical, thermal, and/or chemical stresses, an m-PMSM can potentially develop an incipient ITSC, but the conventional protection might not work properly, or the machine might keep on running while the temperature of the phase affected by shorted turns would reach excessive values to cause critical insulation breakdown. Thus, the stator winding symmetry of the PMSM is lost due to ITSC; phase currents are no more balanced with possible excessive overcurrent conditions, leading to a negative-sequence current circulation, which considerably penalise the motor behaviour. It is worth noting that under such conditions, three-phase or m-PMSMs are potentially subjected to different types of irreversible demagnetisation [7–9].

Hence, ITSC detection at an early stage is required, which may not only eliminate the subsequent damage propagation to adjacent coils and the stator core, but also reduces repair costs and improves the availability of the machine considerably.

For the detection of an ITSC in three-phase PMSMs, a large variety of approaches have been proposed. Effective off-line tests, such as stator winding resistance asymmetry measurements, partial discharge analysis (PDA), or infrared thermography (IT), have been successfully adopted [10]. In order to avoid dedicated equipment, spectral analysis of current or voltage space-vectors (SVs), as well as the corresponding negative or zero-sequence components analysis, have been successfully investigated for ensuring on-line monitoring of stator winding state in three-phase machines [11, 12].

With reference to m-PMSMs, it is well known that even if one or more phases are opened due to stator failures, the remaining healthy phases allow the motor to operate with a degraded mode [13, 14]. Thus, several fault-tolerant control approaches, against stator asymmetries or inverter related faults, have been the target of large research efforts [15–18], in order to guarantee reliable operating conditions and thus reducing unexpected failures. However, dedicated solutions for stator winding anomalies detection are still under investigation [19–23].

In [19], the proposed approach for stator fault diagnosis is based on stator current positive- and negative-sequence fundamental components expressed in the stationary α–β reference frame. The

evaluated values are used for computing a fault index for detecting stator open-circuit faults. Based on particle swarm optimisation (PSO), a parameter estimation method is presented in [20], where a fitness function representative of an ITSC is proposed for detecting and quantifying the fault level in five-phase PMSMs. Stator ITSC detection by reactive power in dual three-phase reluctance motors is presented in [21], where a differential diagnostic index is defined for effective diagnosis of the fault. In [22], the stator currents and zero-sequence voltage components (ZSVCs) harmonics are investigated for developing a fault diagnosis scheme based on the changes in their spectral content. When compared to the use of stator currents spectra analysis, the same reference has shown that the ZSVC-based method shows better performance with higher sensitivity. An improved control architecture that provides an efficient on-line detection and discrimination of demagnetisation and stator resistance unbalance, and ensure a nearly undisturbed behaviour of a 5-PMSM was developed in [18]. In this context, an important issue that cannot be ignored, is that the detectability of stator winding anomalies is particularly dependent on the windings design of the machine. This fact was experimentally examined by Bianchi *et al.* [24] for a 5-PMSM. Thus, the implementation of stator fault monitoring systems dedicated to m-PMSMs should consider the winding design of the machine.

Recently, the spectral analysis of the back-emf SVs, evaluated in the different α–β subspaces, have been investigated in [23], where potential harmonics chain has been identified as the relevant fault signature for stator winding ITSC detection in 6-PMSMs. However, the relevance of the fault signature for real power generation systems, where such machines operate in closed-loop conditions, requires further investigations. In this context, the identified fault signature for detecting ITSC in 6-PMSM [23], is here further investigated and tracked by current spectral analysis (CSA) and voltage spectral analysis (VSA).

In this paper, the assessment of a stator winding ITSC detectability, by back-emf in open-loop condition, and then by CSA and VSA in closed-loop condition, is completely supported by experiments.

In Section 2, the mathematical model of the 6-PMSM is presented according to the multiple SV representation concept, where the spectral analysis of the back-emfs is emphasised. The reliability of an ITSC fault signature, based on back-emf SVs analysis, is verified by finite element analysis (FEA) simulations and experimental tests in Section 3. Then, in Section 4, the adopted control system for 6-PMSMs and the experimental setup is illustrated, whereas the results of the experimental tests are included in Section 5. Finally, the conclusions are depicted in Section 6.

2 Mathematical model of 6-PMSMs

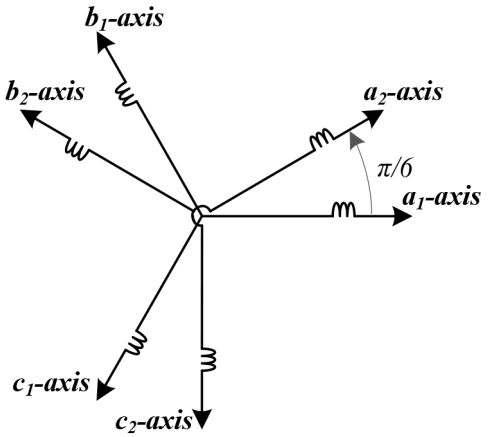

Fig. 1 *Schematic diagram of the 6-PMSM windings with separate neutral points*

2.1 Six-phase systems representation based on multiple SV concept

For a given electrical system, represented by six real quantities x_{a1}, x_{a2}, x_{b1}, x_{b2}, x_{c1}, x_{c2}, as presented in Fig. 1 for a 6-PMSM, a new system composed of three SVs can be obtained as

$$\bar{\boldsymbol{y}}_{\alpha k-\beta k} = \boldsymbol{y}_{\alpha k} + j\boldsymbol{y}_{\beta k}; \quad k = 1, 3, 5, \ldots \tag{1}$$

where the vector components $(\boldsymbol{y}_{\alpha k})_{k=1,3,5}$ and $(\boldsymbol{y}_{\beta k})_{k=1,3,5}$ are calculated as

$$\begin{bmatrix} y_{\alpha 1} \\ y_{\beta 1} \\ y_{\alpha 3} \\ y_{\beta 3} \\ y_{\alpha 5} \\ y_{\beta 5} \end{bmatrix} = \frac{1}{2}\begin{bmatrix} 1 & -1/2 & -1/2 & \sqrt{3}/2 & -\sqrt{3}/2 & 0 \\ 0 & \sqrt{3}/2 & -\sqrt{3}/2 & 1/2 & 1/2 & -1 \\ 1 & 1 & 1 & 0 & 0 & 0 \\ 0 & 0 & 0 & 1 & 1 & 1 \\ 1 & -1/2 & -1/2 & -\sqrt{3}/2 & \sqrt{3}/2 & 0 \\ 1 & -\sqrt{3}/2 & \sqrt{3}/2 & 1/2 & 1/2 & -1 \end{bmatrix}\begin{bmatrix} x_{a1} \\ x_{b1} \\ x_{c1} \\ x_{a2} \\ x_{b2} \\ x_{c2} \end{bmatrix} \tag{2}$$

In fact, by assuming the obtained three new complex vectors expressed by (1) as of current SVs, the subscripts 1, 3, 5 are corresponding to the order of the main harmonic, they produce in the resulting magnetic-field distribution.

By additional analytical developments, one can easily verify that the secondary harmonics in the magnetic-field distribution are corresponding to the 11th, 9th, and 7th order, respectively [25].

2.2 SVs harmonic content analysis

Multiple SV representation is very practical for multiphase systems description and analysis [26], as it is possible to elaborate an SV modelling of 6-PMSMs on three different α–β subspaces [27]. The considered machine is a 30° asymmetrical 6-PMSM, whose neutral points are separated, as presented in Fig. 1.

Considering the adopted stator winding configuration (Fig. 1), the resulting formulation of the 6-PMSM model in terms of multiple SVs representation can be obtained

$$\bar{v}_{Sk} = R_S\bar{i}_{Sk} + \frac{\mathrm{d}\bar{\phi}_{Sk}}{\mathrm{d}t}; \quad k = 1, 3, 5, \ldots \tag{3}$$

where the SVs of the linkage fluxes $\bar{\phi}_{S1}, \bar{\phi}_{S3}, \bar{\phi}_{S5}$ are given by

$$\begin{aligned}\bar{\phi}_{S1} = {} & L_{S1}\bar{i}_{S1} + 2\varphi_{M1}\cos(\gamma)\, e^{j\theta} \\ & + 2\varphi_{M11}\cos(11\gamma)\, e^{-j11\theta},\end{aligned} \tag{4}$$

$$\begin{aligned}\bar{\phi}_{S3} = {} & L_{S3}\bar{i}_{S3} + 2\varphi_{M3}\cos(3\gamma)\, e^{j3\theta} \\ & + 2\varphi_{M9}\cos(9\gamma)\, e^{-j9\theta},\end{aligned} \tag{5}$$

$$\begin{aligned}\bar{\phi}_{S5} = {} & L_{S5}\bar{i}_{S5} + 2\varphi_{M5}\cos(5\gamma)\, e^{j5\theta} \\ & + 2\varphi_{M7}\cos(7\gamma)\, e^{-j7\theta}.\end{aligned} \tag{6}$$

In (4)–(6), θ is the relative position between stator and rotor in electrical radians, $\gamma = (\pi - \beta)/2$ and β is the magnet pole arc in electrical radians, whereas L_{S1}, L_{S3}, and L_{S5} are the α_1–β_1, α_3–β_3, and α_5–β_5 synchronous inductances [25].

Considering the α_1–β_1, α_3–β_3, and α_5–β_5 SVs of the fluxes linked with stator windings, given by the expressions (4)–(6), the efficient stator windings ITSC detection can be based on frequency analysis of the following back-emf SVs:

$$\begin{aligned}\bar{e}_{S1} = {} & 2j\omega\varphi_{M1}\cos(\gamma)\, \mathrm{e}^{j\theta} \\ & - 22j\omega\varphi_{M11}\cos(11\gamma)\, \mathrm{e}^{-j11\theta},\end{aligned} \tag{7}$$

$$\begin{aligned}\bar{e}_{S3} = {} & 6j\omega\varphi_{M3}\cos(3\gamma)\, \mathrm{e}^{j3\theta} \\ & - 18j\omega\varphi_{M9}\cos(9\gamma)\, \mathrm{e}^{-j9\theta},\end{aligned} \tag{8}$$

Table 1 Parameters of the 6-PMSM

Parameter		
phase resistance	0.36	Ω
pole number	4	—
phase inductance	1.44	mH
stator inner radius	150	mm
stator outer radius	240	mm
slot number	48	—
stator winding pitch	165°	el. degrees
magnet pole-arc	151°	el. degrees
magnet radial thickness	5	mm

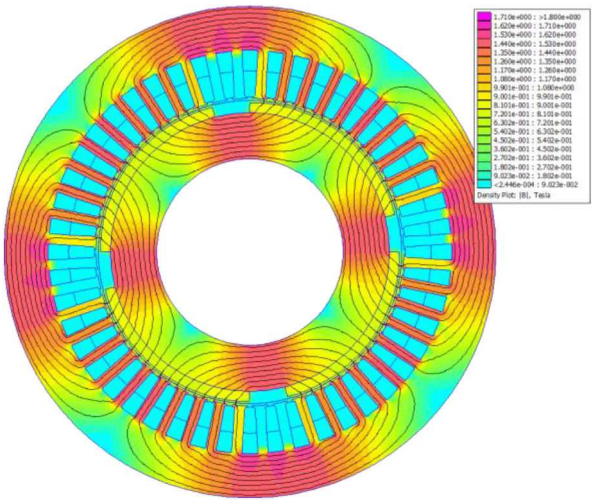

Fig. 2 *Cross-section of the healthy 6-PMSM*

$$\begin{aligned}\bar{e}_{S5} = {} & 10j\omega\varphi_{M5}\cos(5\gamma)\,\mathrm{e}^{j5\theta} \\ & -14j\omega\varphi_{M7}\cos(7\gamma)\,\mathrm{e}^{-j7\theta}.\end{aligned} \tag{9}$$

where the constant values φ_{M1}, φ_{M3}, φ_{M5}, φ_{M7}, φ_{M9}, and φ_{M11} can be expressed as

$$\varphi_{M1} = \frac{2\mu_0 N_S L\tau H_{R,\max} K_{BS1} K_{RS1}}{\pi^2}, \tag{10}$$

$$\varphi_{M3} = \frac{2\mu_0 N_S L\tau H_{R,\max}}{\pi^2}\frac{K_{BS3} K_{RS3}}{9}, \tag{11}$$

$$\varphi_{M5} = \frac{2\mu_0 N_S L\tau H_{R,\max}}{\pi^2}\frac{K_{BS5} K_{RS5}}{25}, \tag{12}$$

$$\varphi_{M7} = \frac{2\mu_0 N_S L\tau H_{R,\max}}{\pi^2}\frac{K_{BS7} K_{RS7}}{49}, \tag{13}$$

$$\varphi_{M9} = \frac{2\mu_0 N_S L\tau H_{R,\max}}{\pi^2}\frac{K_{BS9} K_{RS9}}{81}, \tag{14}$$

$$\varphi_{M11} = \frac{2\mu_0 N_S L\tau H_{R,\max}}{\pi^2}\frac{K_{BS11} K_{RS11}}{121}. \tag{15}$$

Observing (7)–(9), the spectral content of the back-emf SVs in the α_1–β_1 and α_5–β_5 subspaces, can be identified for healthy conditions. Considering (7), the back-emf SV evaluated in the plane α_1–β_1 shows only the 1st and the 11th harmonic components.

The spectral content of the back-emf SV in the plane α_3–β_3 is composed by the 3rd and the 9th harmonic components (see (8)), whereas the back-emf SV in the plane α_5–β_5 is based on the contribution of the 5th and the 7th harmonic components (see (9)). Thus, the reference diagnosis for a healthy condition is clearly identified in the α_1–β_1, α_3–β_3, and α_5–β_5 subspaces.

By considering a power balance, and taking into account the previous equations, the electromagnetic torque can be expressed by

$$T_{\mathrm{em}} = T_{\mathrm{em.1}} + T_{\mathrm{em.3}} + T_{\mathrm{em.5}} + T_{\mathrm{em.7}} + T_{\mathrm{em.9}} + T_{\mathrm{em.11}}, \tag{16}$$

where

$$T_{\mathrm{em.1}} = 6p\varphi_{M1}\left[\bar{i}_{S1}\cdot j\cos(\gamma)\mathrm{e}^{j\theta}\right], \tag{17}$$

$$T_{\mathrm{em.3}} = 18p\varphi_{M3}\left[\bar{i}_{S3}\cdot j\cos(3\gamma)\mathrm{e}^{j3\theta}\right], \tag{18}$$

$$T_{\mathrm{em.5}} = 30p\varphi_{M5}\left[\bar{i}_{S5}\cdot j\cos(5\gamma)\mathrm{e}^{j5\theta}\right], \tag{19}$$

$$T_{\mathrm{em.7}} = 42p\varphi_{M7}\left[\bar{i}^{*}_{S5}\cdot j\cos(7\gamma)\mathrm{e}^{j7\theta}\right], \tag{20}$$

$$T_{\mathrm{em.9}} = 54p\varphi_{M9}\left[\bar{i}^{*}_{S3}\cdot j\cos(9\gamma)\mathrm{e}^{j9\theta}\right], \tag{21}$$

$$T_{\mathrm{em.11}} = 66p\varphi_{M11}\left[\bar{i}^{*}_{S1}\cdot j\cos(11\gamma)\mathrm{e}^{j11\theta}\right]. \tag{22}$$

where the symbols '*' and '.' identify the complex conjugate quantities and the scalar product, respectively.

The electromagnetic torque, expressed by (16), is the sum of six contributions, where each one can be identified by the corresponding harmonic order in the flux linkage. Two of them are related to the current space vector $\bar{i}_{S1}$, the second pair is related to the third current space vector $\bar{i}_{S3}$, and the remaining pair is related to the fifth current space vector $\bar{i}_{S5}$.

Considering the adopted stator winding design of the machine, with isolated neutral points, the contributions $T_{\mathrm{em.3}}$ and $T_{\mathrm{em.9}}$, related to the third current space vector $\bar{i}_{S3}$, are equal to zero.

The three contributions of $T_{\mathrm{em.5}}$, $T_{\mathrm{em.7}}$ and $T_{\mathrm{em.11}}$ can cause undesired torque pulsations. In order to obtain a smooth torque waveform, it is possible to set $\bar{i}_{S5}$ to zero, together with a proper machine design, ensuring a negligible value of φ_{M11}.

3 Validation of motor signal-based detection technique of ITSC

In the present section, the proposed ITSC fault signature is firstly based on back-emf SVs analysis in no-load operating conditions. The performance of this approach is preliminarily explored by FEA, then validated by experiments.

3.1 FEA results

In order to validate the theoretical analysis of the back-emf spectral content, the simulation of a 6-PMSM has been carried out using FEA [23].

The main machine parameters are presented in Table 1. Four poles, 48 slots, double-layer, short pitch stator windings, having two slots per pole and per phase, was considered.

The cross-section of the healthy 6-PMSM, with a typical flux plot obtained by 2D FEA, under no-load conditions, is depicted in Fig. 2.

Based on the previous torque analysis, it is clear that in order to reduce the undesired torque ripple contributions, the 11th harmonic component of the flux linked with stator windings should be minimised (see (22)). This can be practically achieved by using a stator winding pitch of 165°.

The cogging torque contribution is not included in (16); therefore the guidelines followed for the design were based on selecting the appropriate angle for the magnet pole arc for achieving a trade-off solution between the need to minimise the cogging torque and to compensate, as much as possible, the effects of the 5th and 7th harmonics of the flux linkage.

The analysis has been carried out using FEA and the results obtained for the cogging torque are illustrated in Fig. 3. This figure shows the peak to peak values of the cogging torque as a function of the magnet pole arc, expressed in mechanical degrees.

The minimum for the cogging torque is obtained for a pole arc value around 75°. The value of 75.5° mechanical degrees (corresponding to 151° electrical degrees) has been selected because this value is the one which ensures a satisfactory compensation of 5th and 7th harmonics of the flux linkage. Fig. 4 shows the magnitude of 5th and 7th harmonics as a function of the magnet pole arc calculated by FEA, and the magnitude of the same harmonics for the pole arc equal to 75.5° measured on the prototype. As it is possible to note, the 5th harmonic of the flux linkage is practically zero, and the 7th is not zero but shows a reduced value.

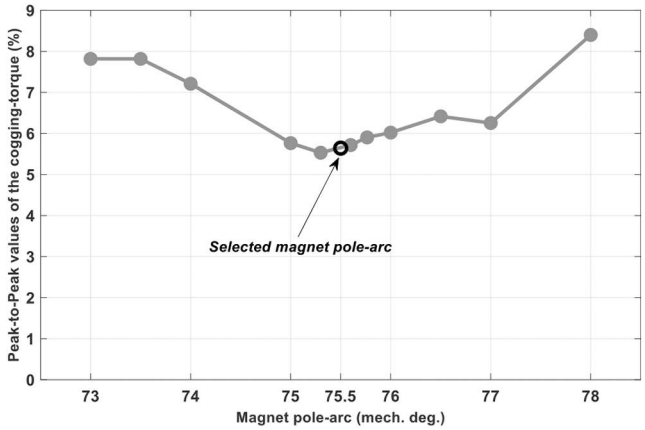

Fig. 3 *FEA: the peak-to-peak values of the cogging-torque according to the magnet pole-arc values*

The fluxes linked with the stator windings obtained by FEA have been imported in the MATLAB® environment for back-emfs calculation and data computing in the different α–β planes. For accurate analysis of the investigated fault signature, the back-emfs have been normalised by the mechanical speed (expressed in rad/s) for obtaining the well-known 'normalised back-emf'.

When an ITSC occurs in a stator phase winding, a certain number of turns will not give their contribution to the back-emf, then leading to a reduction of the total back-emf in the faulty phase. The FEA has been carried out under this assumption.

A case study has been considered, in which the fault is assumed to involve 12.5% of the total number of turns per phase, thus determining a 12.5% amplitude attenuation of the back-emf in the faulty phase a_1 (Fig. 1).

Figs. 5*a* and *b* show the spectra of the back-emfs SV for healthy conditions, evaluated in the α_1–β_1, and α_5–β_5 planes, respectively.

Fig. 6*a* shows the harmonic spectrum of the back-emfs SV in the α_1–β_1 plane, for the simulated ITSC. By comparing the obtained spectra for healthy (Fig. 5*a*), and faulty (Fig. 6*a*) conditions, the magnitude evolution of the inverse component at $-f$ is clearly verified, which is classically expected in the α_1–β_1 plane, leading to a first spectral fault signature of the ITSC.

The harmonic spectrum of the back-emfs SV, evaluated in the α_5–β_5 plane for ITSC fault, is depicted in Fig. 6*b*. With reference to the healthy case (Fig. 5*b*), the magnitude variation of the fault components at $\pm f$ and $\pm 3f$ is clearly evidenced, leading to a second more relevant spectral fault signature of the ITSC. The 5th and 7th harmonics due to the magnet pole arc design are unchanged.

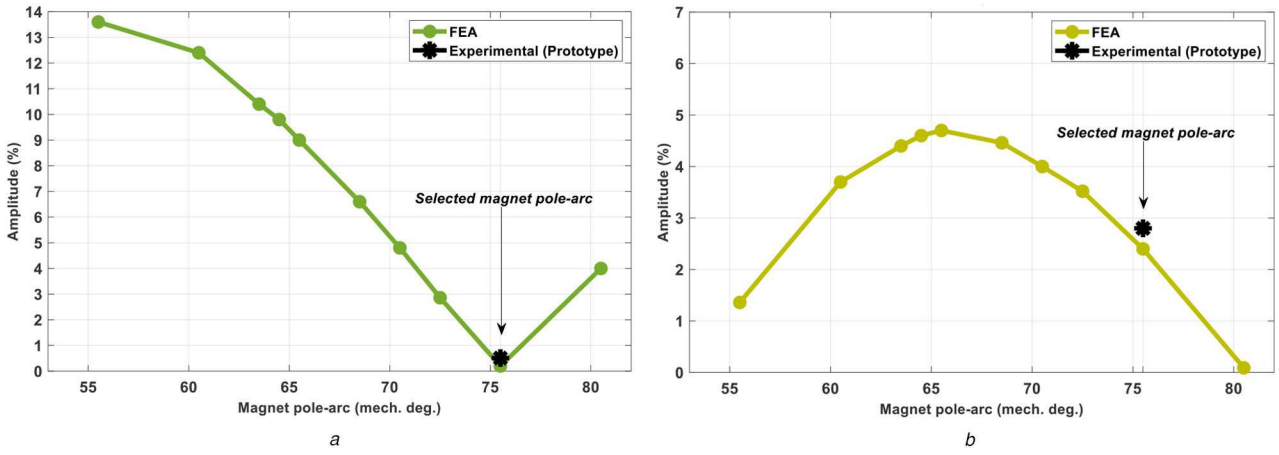

Fig. 4 *Amplitudes of*
(a) 5th and ***(b)*** 7th harmonics of the flux linkage according to the magnet pole-arc values

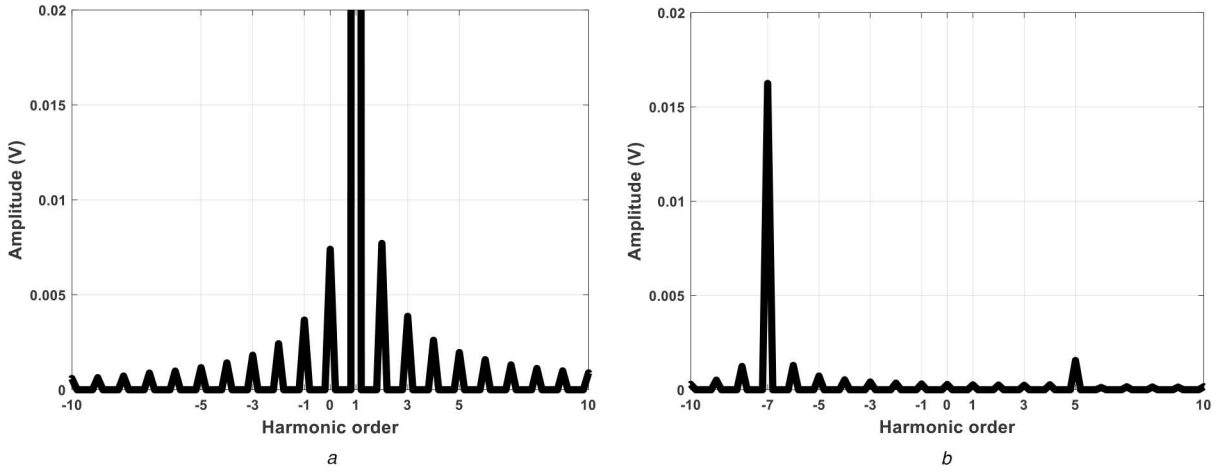

Fig. 5 *FEA: spectra of the back-emfs SV in*
(a) α_1–β_1 plane and ***(b)*** α_5–β_5 plane for a healthy machine

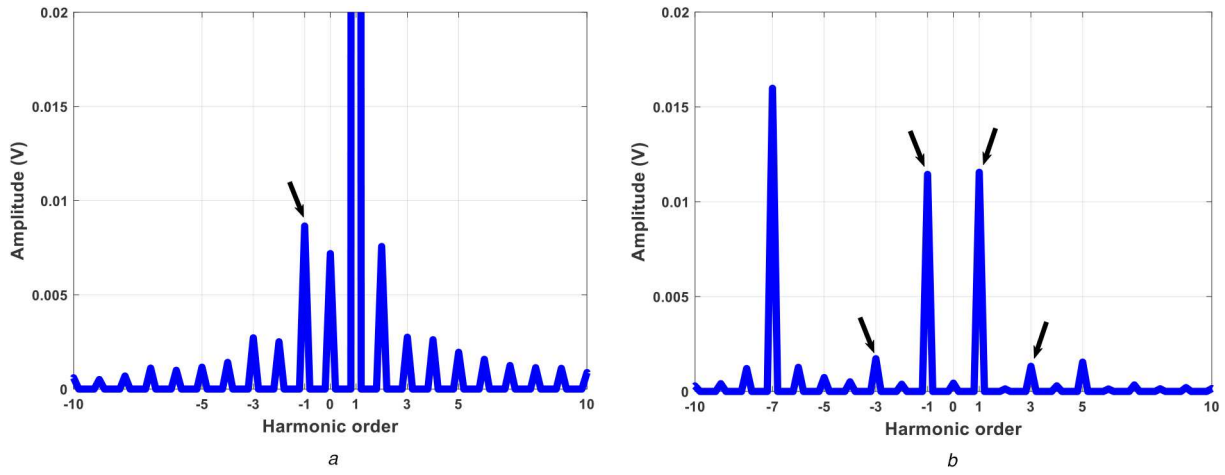

Fig. 6 *FEA: spectra of the back-emfs SV in*
(a) α_1–β_1 plane and ***(b)*** α_5–β_5 plane under faulty conditions. The fault was emulated by a 12.5% amplitude attenuation applied to phase-a_1

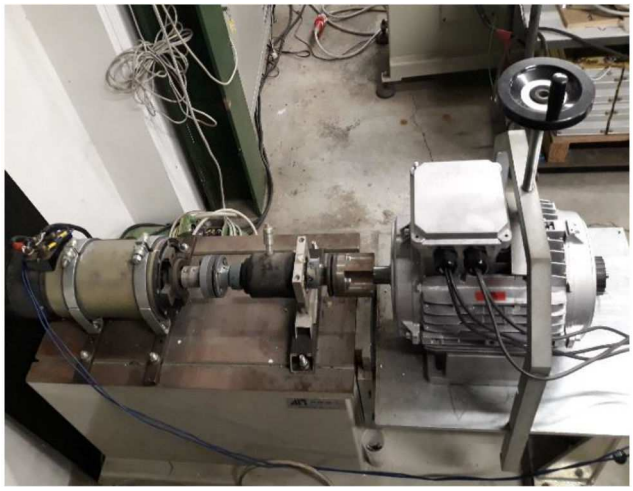

Fig. 7 *Experimental test bench*

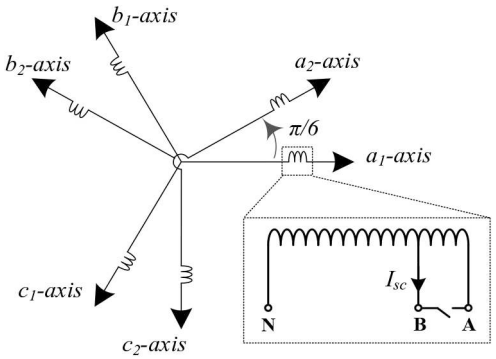

Fig. 8 *Schematic diagram of the 6-PMSM prototype with ITSC in phase-a_1*

3.2 Experimental validation

To validate the spectral ITSC fault signatures, previously identified in the SV of the back-emfs in the α_1–$\beta_1$and α_5–β_5 planes, a prototype of a 6-PMSM with the same geometry and parameters used in the simulation (Table 1), has been built for experimental tests (Fig. 7). A set of winding turns in phase-a_1 is accessible for introducing a real ITSC involving 12.5% of the phase winding turns, as presented in Fig. 8.

The machine was driven by a 9-kW DC motor, fed by a commercial speed-controlled DC/DC converter that acts as a prime mover. The back-emfs were recorded by an oscilloscope, with a sampling frequency of 50 kHz. Then, the signals were imported in the MATLAB® environment for calculating SVs in the α_1–β_1 and α_5–β_5 planes, and corresponding spectral treatments.

For a precise experimental evaluation of the tracked ITSC fault signature, the back-emfs were normalised by the mechanical speed (expressed in rad/s), in the time domain. For the same purposes, the computed spectra evaluated in the α_1–β_1 and α_5–β_5 planes, have been normalised with the 1st and the −7th harmonic components magnitudes, respectively.

Initially, the machine is operating with healthy six-phase stator windings at rated speed (1000 rpm). The obtained spectra of the back-emfs SV, in the α_1–β_1 and α_5–β_5 planes, are depicted in Figs. 9*a* and *b*, respectively. As can be seen, the obtained experimental harmonic mapping into the α_1–β_1 and α_5–β_5 planes for the healthy machine, apart from unavoidable noise of a real machine, corroborate simulations obtained by FEA (Fig. 5). In particular, the 5th and 7th harmonics due to the magnet pole arc design are still evident.

The spectra of the back-emfs SV in the α_1–β_1 and α_5–β_5 planes, in the presence of ITSC, are reported in Figs. 10*a* and *b*, respectively. Comparing the spectra of Figs. 10*a* and 6*a*, to the corresponding spectra for healthy condition, we can note a similar amplitude variation of harmonic at−*f*, and the presence of new harmonics due to the short-circuit current in phase a_1, which affects the magnetic field distribution and then back-emfs [23].

With reference to the faulty case with ITSC, Fig. 10*b* shows the presence of a higher number of harmonics with respect to FEA results in Fig. 6*b*, which is justified by the real short-circuit current in phase a_1. Nevertheless, Fig. 10*b* clearly illustrates a relevant amplitude variation of the harmonics at ±*f*, ±3*f*, as in Fig. 6*a*, validating what anticipated by FEA.

The introduced ITSC has caused a relevant amplitude variation of the fault harmonic components at−*f* in the α_1–β_1 plane and ±*f*, ±3*f* in the α_5–β_5 planes. As a final comment, we can conclude that the amplitude variations of the fault harmonic components in the α_5–β_5 plane are more significate and useful for synthetising a reliable stator winding ITSC fault index for 6-PMSMs.

4 Control system for 6-PMSMs and experimental implementation

A field-oriented control (FOC) strategy is adopted to implement a closed-loop speed control of the 6-PMSM (Fig. 11). Taking into account the transformation (2), and considering the stator windings design with isolated neutral points, the current SV in the plane α_3–β_3 is equal to zero. Thus, after substituting (4)–(6) into (3), the formulation of the voltage equations expressed in the stator reference frame, can be limited to the first and fifth subspaces, leading to

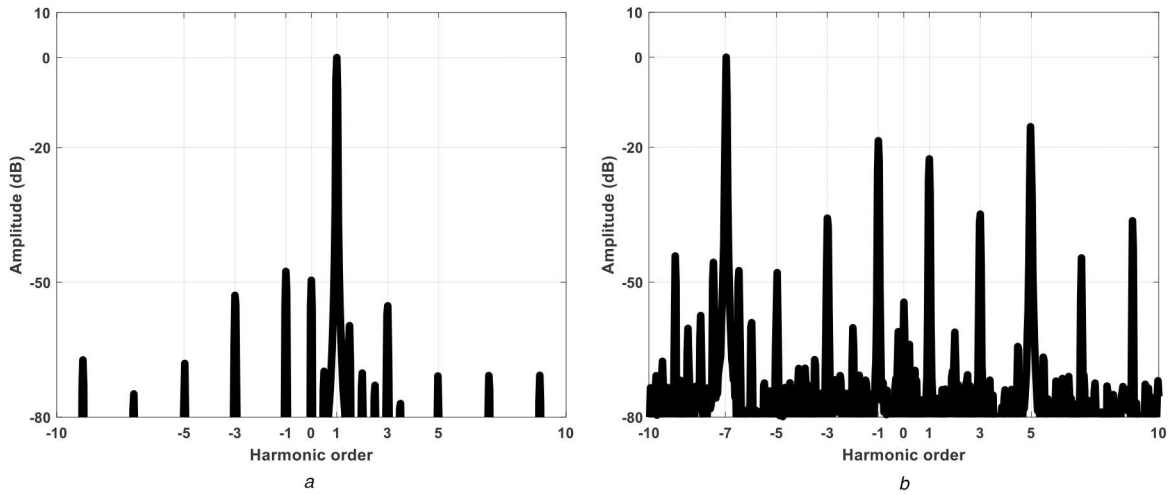

Fig. 9 *Experimental test: spectra of the back-emf SVs in* ***(a)*** α_1–β_1 plane and ***(b)*** α_5–β_5 plane for a healthy machine

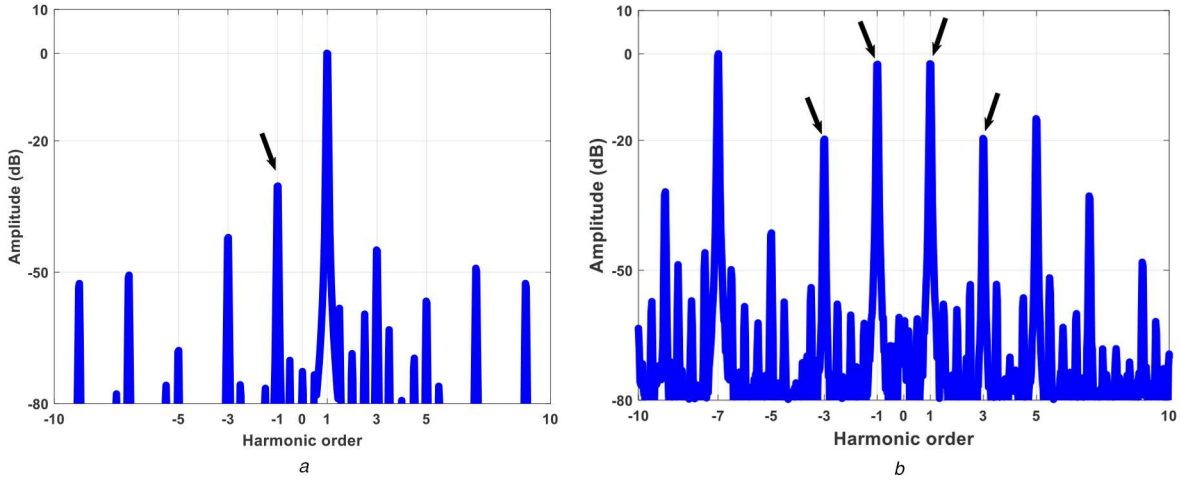

Fig. 10 *Experimental test: spectra of the back-emf SVs in* ***(a)*** α_1–β_1 plane and ***(b)*** α_5–β_5 plane under a real 12.5% of ITSC in phase-a_1

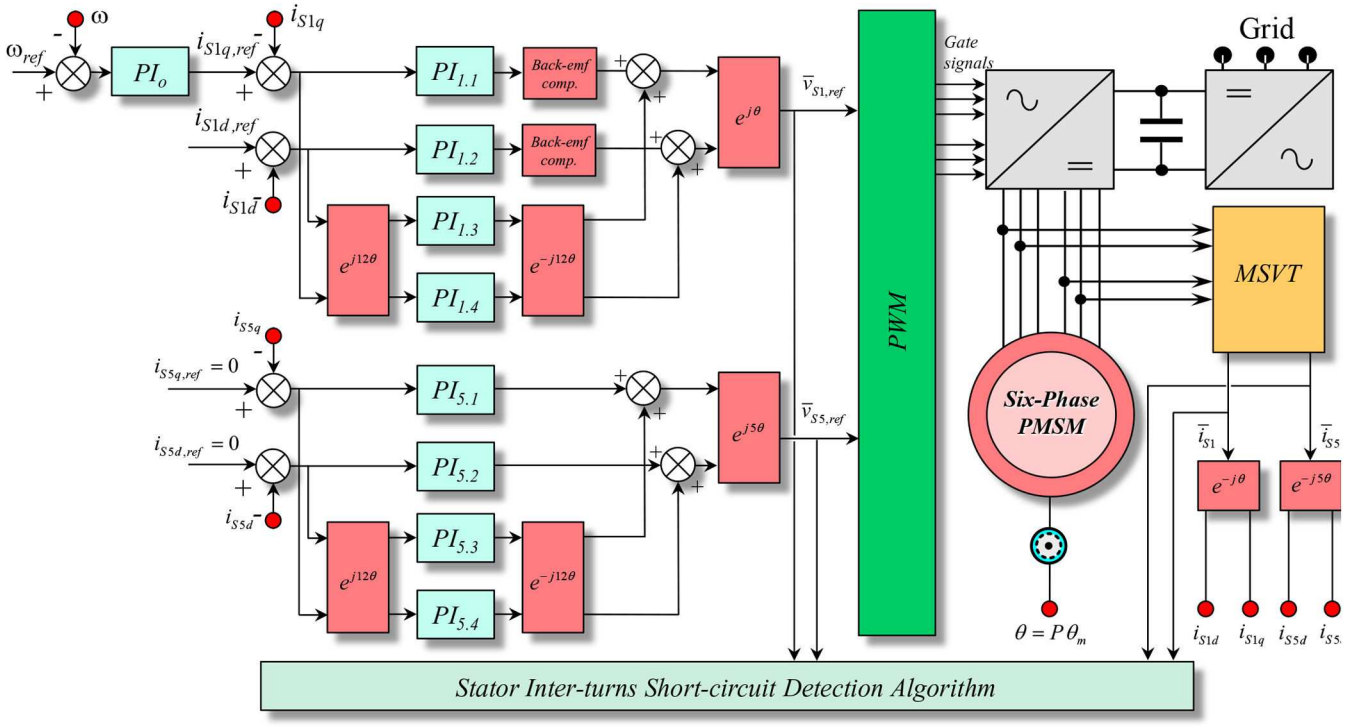

Fig. 11 *Vector-control of the six-phase AC permanent magnet motor drive*

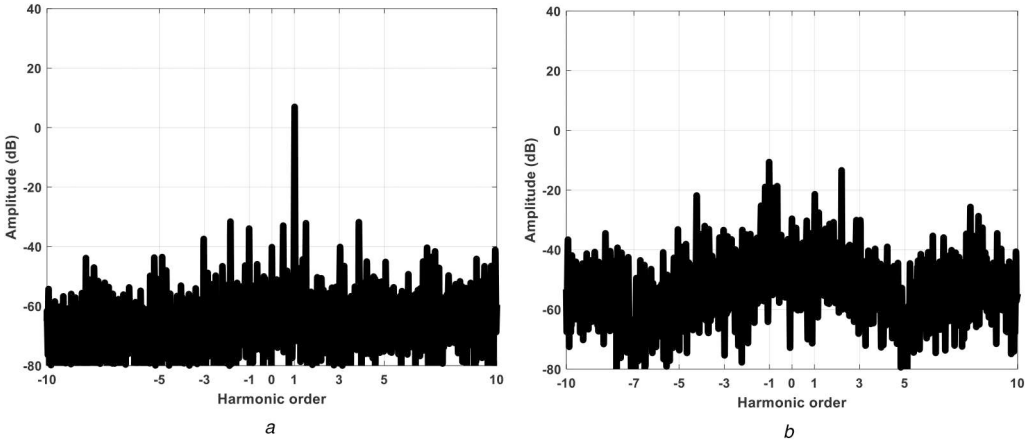

Fig. 12 *Experimental test: spectra based on CSA in* ***(a)*** α_1–β_1 plane and ***(b)*** α_5–β_5 plane for a healthy machine

$$\bar{v}_{S1} = R_S\bar{\boldsymbol{i}}_{S1} + L_{S1}\frac{\mathrm{d}\bar{\boldsymbol{i}}_{S1}}{\mathrm{d}t} + j\omega\varphi_{m1}\mathrm{e}^{j\theta} - j11\omega\varphi_{m11}\mathrm{e}^{-j11\theta}, \tag{23}$$

$$\bar{v}_{S5} = R_S\bar{\boldsymbol{i}}_{S5} + L_{S5}\frac{\mathrm{d}\bar{\boldsymbol{i}}_{S5}}{\mathrm{d}t} + j5\omega\varphi_{m5}\mathrm{e}^{j5\theta} - j7\omega\varphi_{m7}\mathrm{e}^{-j7\theta}, \tag{24}$$

where $w = dq/dt$, and the constant quantities φ_{m1}, φ_{m5}, φ_{m7}, and φ_{m11} are given by

$$\varphi_{m1} = 2\varphi_{M1}\cos(\gamma), \tag{25}$$

$$\varphi_{m5} = 2\varphi_{M5}\cos(5\gamma), \tag{26}$$

$$\varphi_{m7} = 2\varphi_{M7}\cos(7\gamma), \tag{27}$$

$$\varphi_{m11} = 2\varphi_{M11}\cos(11\gamma)\,. \tag{28}$$

In order to implement the FOC strategy, shown in Fig. 11, it is useful to reformulate the machine voltage equations in the rotating reference frames.

The equations regarding the components in the d_1–q_1 plane are written in a reference frame rotating at an angular speed of ω, whereas the equations concerning the d_5–q_5 plane are written in a reference frame rotating at an angular speed of 5ω. The transformation from the rotor reference frame to the stator reference frame (and vice versa) can be expressed by

$$\bar{y}_1^r = \bar{y}_1\mathrm{e}^{-j\theta} \tag{29}$$

$$\bar{y}_5^r = \bar{y}_5\mathrm{e}^{-j5\theta} \tag{30}$$

where $\bar{y}_1^r$ and $\bar{y}_5^r$ are the variables in the new rotating reference frames, $\bar{y}_1$ and $\bar{y}_5$ are the same variables in the stationary reference frames. Considering (29) and (30), for (23) and (24), respectively, leads to

$$\begin{aligned}\bar{v}_{S1}^r = {} & R_S\bar{i}_{S1}^r + L_{S1}\frac{\mathrm{d}\bar{i}_{S1}^r}{\mathrm{d}t} + j\omega L_{S1}\bar{i}_{S1}^r \\ & + j\omega\varphi_{m1} - j11\omega\varphi_{m11}\mathrm{e}^{-j12\theta}\end{aligned} \tag{31}$$

$$\begin{aligned}\bar{v}_{S5}^r = {} & R_S\bar{i}_{S5}^r + L_{S5}\frac{\mathrm{d}\bar{i}_{S5}^r}{\mathrm{d}t} + j\omega L_{S5}\bar{i}_{S5}^r \\ & + j5\omega\varphi_{m5} - j7\omega\varphi_{m7}\mathrm{e}^{-j12\theta}\end{aligned} \tag{32}$$

To ensure an effective current tracking, considering the disturbing effects of the back-emfs and according to (31) and (32), eight current regulators have been implemented in four different reference frames. $PI_{1.1}$ and $PI_{1.2}$ are employed on the d_1–q_1 reference frame rotating at an angular speed equal to ω. $PI_{5.1}$ and $PI_{5.2}$ are employed on the d_5–q_5 reference frame rotating at an angular speed equal to 5ω. Finally, $PI_{1.3}$, $PI_{1,4}$ and $PI_{5.3}$, $PI_{5.4}$, are employed in reference frames synchronous with the eleventh harmonic and the seventh harmonic of the back-emfs, respectively.

Consequently, at a steady state, the expected spectrum of the current space vector $\bar{\boldsymbol{i}}_{S1}$ should not contain the residual −11th harmonic thanks to the short pitch stator windings design and features of the current regulator implemented. In addition, the 5th and the−7th harmonics should be zero in the spectrum of the current space vector $\bar{\boldsymbol{i}}_{S5}$ thanks to the features of the current regulator implemented.

The reference current $i_{SIq,\mathrm{ref}}$ is obtained by the regulator PI_o of the outer speed loop. The reference voltage space vectors $\bar{\boldsymbol{v}}_{S1,\mathrm{ref}}$, and $\bar{\boldsymbol{v}}_{S5,\mathrm{ref}}$ are calculated exploiting the outputs of the eight current regulators, by means of proper coordinate transformations.

In order to track experimentally the stator CSA and VSA introduced by the ITSC back-emf harmonic components at $-f$ in the α_1–β_1 plane and $\pm f$, $\pm 3f$ in the α_5–β_5 planes, an experimental benchmark has been installed in the laboratory. The 6-PMSM was now loaded by the same DC motor, with the same controlled converter. A dSPACE® control board has been adopted for implementing the control architecture of Fig. 11. The inverter switching frequency was fixed to 8 kHz with a dead time of 2 µs.

The harmonic spectra were obtained by applying the FFT algorithm to the SVs, evaluated in the α_1–β_1 and α_5–β_5 planes, of the monitored variables (both currents and voltages). For accurate spectral analysis, a high sampling rate of 100 kHz was adopted for all data acquisitions.

5 Results

As established in the previous section, based on specific harmonic components in the stator back-emfs, a highly sensitive fault index for stator ITSC detection can be established in no-load conditions. The present section is dedicated to the assessment of the ITSC fault signature, under closed-loop vector-controlled 6-PMSM conditions, using CSA and VSA.

All the experimental tests have been conducted at a constant speed of 500 rpm, with a load torque of 8 Nm.

Initially, the 6-PMSM was run in healthy conditions, then under ITSC of phase a_1, where 12.5% of the total number of turns per phase was short circuited (Fig. 8).

5.1 Current signature analysis in the α–β planes

The reference spectra of the CSA corresponding to the healthy machine evaluated in the α_1–β_1 and α_5–β_5 planes, are reported in Figs. 12*a* and *b*, respectively. The obtained experimental spectrum in healthy conditions, using CSA evaluated in the α_1–β_1 (Fig. 12*a*) corroborate to the spectral content of the back-emfs SV evaluated in the same plane (Fig. 9*a*), leading to a clear diagnosis of the

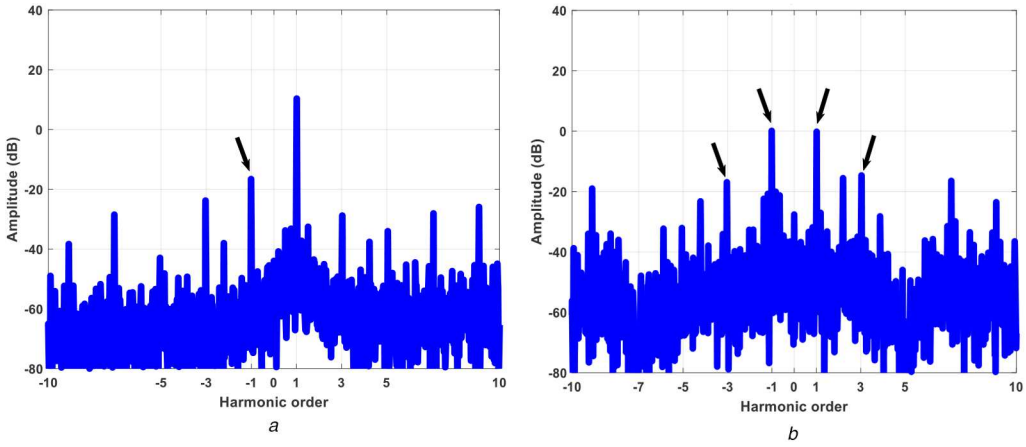

Fig. 13 *Experimental test: spectra based on CSA in*
(a) α_1–β_1 plane and ***(b)*** α_5–β_5 plane for a real 12.5% of ITSC in phase-a$_1$

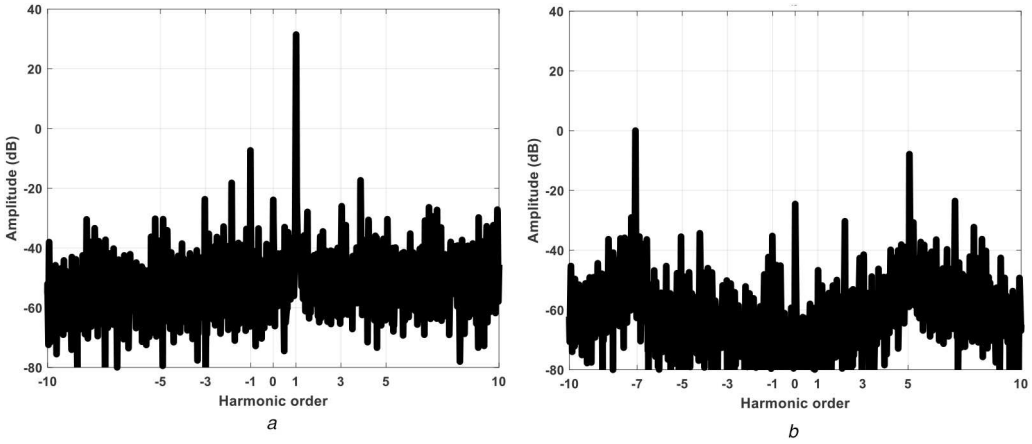

Fig. 14 *Experimental test: spectra based on VSA in*
(a) α_1–β_1 plane and ***(b)*** α_5–β_5 plane for a healthy machine

healthy conditions. Whereas the absence of the $+5$th and -7th harmonics in the spectrum of the CSA in the α_5–β_5 plane, when compared to the spectrum of Fig. 9*b*, is mainly due to the adopted current regulators of Fig. 11, which completely eliminates the contribution of these two harmonic components.

The spectra based on CSA evaluated in the α_1–$\beta_1$and α_5–β_5 planes, for faulty conditions, are reported in Figs. 13*a* and *b*, respectively. Comparing spectra of the CSA in the α_1–β_1 plane, from healthy (Fig. 12*a*) to faulty conditions (Fig. 13*a*), it is evident that the introduced ITSC has caused a relevant magnitude variation of the fault components $-f$, as it could be expected.

However, the corresponding spectra in the α_5–β_5 plane, under healthy conditions and 12.5% of ITSC in phase-a_1, reported in Figs. 12*b* and 13*b*, respectively, show a clear amplitude variation of the fault harmonic components $\pm f$ and $\pm 3f$, leading to a more evident spectral mapping representative of the ITSC fault.

5.2 Voltage signature analysis in the α–β planes

The harmonic mapping under healthy conditions of $\bar{\boldsymbol{v}}_{S1,\mathrm{ref}}$ and $\bar{\boldsymbol{v}}_{S5,\mathrm{ref}}$ is reported in Figs. 14*a* and *b*, respectively. Observing Fig. 14*a*, it can be noted that the fundamental component is the dominant frequency in the $\bar{\boldsymbol{v}}_{S1,\mathrm{ref}}$ spectrum. The spectrum of $\bar{\boldsymbol{v}}_{S5,\mathrm{ref}}$ in Fig. 14*b* is mainly composed of the 5th and the inverse 7th harmonic components, which are generated by the current regulators to compensate the corresponding back-emfs harmonic components for keeping $\bar{i}_{S5,\mathrm{ref}}$ equal to zero. The corresponding spectra under ITSC condition, are reported in Figs. 15*a* and *b*, respectively.

When comparing the resulting spectra based on VSA in the α_1–β_1 plane, from the healthy case (Fig. 14*a*) to faulty conditions (Fig. 15*a*), it is clearly evidenced that the stator ITSC has caused a relevant magnitude variation of the fault component at $-f$.

As far as the variations of the fault components $\pm f$ and $\pm 3f$ of SVs tracked in the α_5–β_5 plane are concerned, their amplitude variations are clearly evidenced from healthy (Fig. 14*b*) to stator ITSC conditions (Fig. 15*b*), leading to an other sensitive ITSC fault signature in 6-PMSMs, similar to that evidenced for CSA.

6 Quantitative evaluations of the tracked ITSC fault signatures

Once the machine state is qualitatively known using CSA or VSA, the quantitative evaluation of the relationship between the fault index value and the severity of stator ITSC is a necessary step to decide about the operability of the machine.

Considering the proposed approaches based on CSA and VSA, the contributions of the ITSC fault components $\pm f$ and $\pm 3f$, have been evaluated in the α_1–β_1 and α_5–β_5 subspaces.

Based on CSA and VSA evaluated in the α_1–β_1 plane, the magnitude variations of the fault components $-f$ and $\pm 3f$, from healthy to 12.5% of ITSC in phase a_1, are reported in Fig. 16. It is clearly evidenced that the fault harmonic components $\pm 3f$, derived from CSA or VSA in the α_1–β_1 plane, have the same sensitivity to the ITSC. However, the contribution of the fault component $-f$ is more relevant using CSA than VSA for the same α_1–β_1 plane.

On the other hand, the amplitude variations from healthy to 12.5% of ITSC in phase a_1, of the fault components $\pm f$ and $\pm 3f$ obtained by CSA and VSA in the α_5–β_5 plane, are represented in Fig. 17. The reported results show clearly that CSA and VSA have the same sensitivity to the stator ITSC.

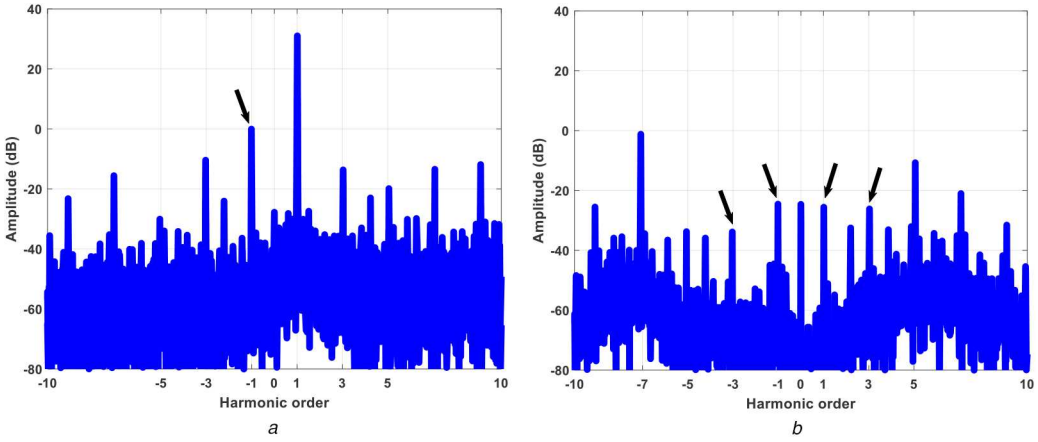

Fig. 15 *Experimental test: spectra based on VSA in* ***(a)*** α_1–β_1 plane and ***(b)*** α_5–β_5 plane for a real 12.5% of ITSC in phase-a_1

Fig. 16 *CSA and VSA evaluated in the α_1–β_1 plane: magnitude variation of the fault components from healthy to 12.5% of ITSC in phase-a_1*

Fig. 17 *CSA and VSA evaluated in the α_5–β_5 plane: magnitude variation of the fault components from healthy to 12.5% of ITSC in phase-a_1*

Finally, considering the contributions of the fault harmonic components evaluated in the two planes α_1–β_1 and α_5–β_5, it was shown that the global fault signature derived from CSA is more sensitive to the ITSC when compared to VSA.

7 Conclusions

In this paper, the experimental assessment of winding ITSC fault signatures in 6-PMSM is presented. The spectral impact of the fault on different variables of the machine is investigated.

The mathematical model presented in the paper is valid only for healthy machines, being its development to include ITSC still under progress. For three-phase machines, these models are already available, but to the best of the author's knowledge, no papers have been published yet for multiphase machines as it is a very demanding problem.

The presented model is anyhow useful because it shows that the diagnosis of ITSC fault can be carried out not only in the plane α_1–β_1, bur more effectively in the plane α_5–β_5.

It was demonstrated that the magnitude variations of fault harmonic components at $\pm f$ and $\pm 3f$, obtained by CSA and VSA in the α_5–β_5 plane, can be considered a highly sensitive diagnostic indicator for detecting an ITSC fault in 6-PMSM.

In addition, this fault signature can be achieved without requiring supplementary hardware, but simply using the already available control signals in α_5–β_5 plane.

Based on the results achieved, the authors are now encouraged to continue the development of the mathematical model for including ITSC faults.

8 References

[1] El-Refaie, A.M.: 'Fault-tolerant permanent magnet machines: a review', *IET Electr. Power Appl.*, 2011, **5**, (1), pp. 59–74

[2] Levi, E.: 'Advances in converter control and innovative exploitation of additional degrees of freedom for multiphase machines', *IEEE Trans. Ind. Electron.*, 2016, **63**, (1), pp. 433–448

[3] Bojoi, R., Cavagnino, A., Cossale, M., *et al.*: 'Multiphase starter generator for a 48-V mini-hybrid powertrain: design and testing', *IEEE Trans. Ind. Appl.*, 2016, **52**, (2), pp. 1750–1758

[4] Wang, X., Wang, Z., Cheng, M., *et al.*: 'Remedial strategies of T-NPC three-level asymmetric six-phase PMSM drives based on SVM-DTC', *IEEE Trans. Ind. Electron.*, 2017, **64**, (9), pp. 6841–6853

[5] Zhou, Y., Chen, G.: 'Predictive DTC strategy with fault-tolerant function for six-phase and three-phase PMSM series-connected drive system', *IEEE Trans. Ind. Electron.*, 2018, **65**, (11), pp. 9101–9112

[6] Toliyat, H.A., Nandi, S., Choi, S., *et al.*: '*Electric machines: modeling, condition monitoring, and fault diagnosis*' (CRC press, USA, 2012)

[7] Faiz, J., Mazaheri-Tehrani, E.: 'Demagnetization modeling and fault diagnosing techniques in permanent magnet machines under stationary and nonstationary conditions: an overview', *IEEE Trans. Ind. Appl.*, 2016, **53**, (3), pp. 2772–2785

[8] Choi, S., Haque, M.S., Tarek, M.T.B., *et al.*: 'Fault diagnosis techniques for permanent magnet ac machine and drives—A review of current state of the art', *IEEE Trans. Transp. Electrif.*, 2018, **4**, (2), pp. 444–463

[9] Gritli, Y., Mengoni, M., Rizzoli, G., *et al.*: 'Rotor magnet demagnetization diagnosis in asymmetrical six-phase surface mounted AC permanent magnet synchronous machine drives', *IET Electr. Power Appl.*, 2019, **14**, (10), pp. 1747–1755

[10] Tallam, R.M., Lee, S.B., Stone, G.C., *et al.*: 'A survey of methods for detection of stator-related faults in induction machines', *IEEE Trans. Ind. Appl.*, 2007, **43**, (4), pp. 920–933

[11] Ben Khader Bouzid, M., Champenois, G., Maalaoui, A., *et al.*: 'Efficient simplified physical faulty model of a permanent magnet synchronous generator dedicated to the stator fault diagnosis part I: faulty model conception', *IEEE Trans. Ind. Appl.*, 2017, **53**, (3), pp. 2752–2761

[12] Yun, J., Lee, K., Lee, K.W., *et al.*: 'Detection and classification of stator turn faults and high-resistance electrical connections for induction machines', *IEEE Trans. Ind. Appl.*, 2009, **45**, (2), pp. 666–675

[13] Fu, J.-R., Lipo, T.A.: 'Disturbance-free operation of a multiphase current-regulated motor drive with an opened phase', *IEEE Trans. Ind. Appl.*, 1994, **30**, (5), pp. 1267–1274

[14] Pant Vinay, G.K.S.: 'Analysis of a multiphase induction machine under fault condition in a phase-redundant AC drive system', *Electr. Mach. Power Syst.*, 2000, **28**, (6), pp. 577–590

[15] Wang, W., Zhang, J., Cheng, M., *et al.*: 'Fault-tolerant control of dual three-phase permanent-magnet synchronous machine drives under open-phase faults', *IEEE Trans. Power Electron.*, 2017, **32**, (3), pp. 2052–2063

[16] Qiu-Liang, H., Yong, C., Li, X.: 'Fault-tolerant control strategy for five-phase PMSM with third-harmonic current injection', *IEEE Access*, 2018, **6**, pp. 58501–58509
[17] Nguyen, N.K., Meinguet, F., Semail, E., *et al.*: 'Fault-tolerant operation of an open-end winding five-phase PMSM drive with short-circuit inverter fault', *IEEE Trans. Ind. Electron.*, 2015, **63**, (1), pp. 595–605
[18] Tani, A., Gritli, Y., Mengoni, M., *et al.*: 'Detection of magnet demagnetization and high-resistance connections in five-phase surface-mounted permanent magnet generators'. Proc. - SDEMPED 2015 IEEE 10th Int. Symp. Diagnostics Electrical Machines Power Electronics Drives, Guarda, Portugal, September 2015, pp. 487–493
[19] Meinguet, F., Semail, E., Gyselinck, J.: 'An on-line method for stator fault detection in multi-phase PMSM drives'. 2010 IEEE Vehicle Power and Propulsion Conf., Lille, France, September 2010, pp. 1–6
[20] Yang, J., Dou, M., Dai, Z., *et al.*: 'Modeling and fault diagnosis of inter-turn short circuit for five-phase PMSM based on particle swarm optimization'. 2016 IEEE Applied Power Electronics Conf. and Exposition (APEC), Long Beach, CA, USA March 2016, pp. 3134–3139
[21] Bianchini, C., Torreggiani, A., Davoli, M., *et al.*: 'Stator fault diagnosis by reactive power in dual three-phase reluctance motors'. 2019 IEEE 12th Int. Symp. on Diagnostics for Electrical Machines, Power Electronics and Drives (SDEMPED), Toulouse, France, August 2019, pp. 251–256
[22] Saavedra, H., Riba, J.-R., Romeral, L.: 'Inter-turn fault detection in five-phase PMSMs. Effects of the fault severity'. in 2013 9th IEEE Int. Symp. on Diagnostics for Electric Machines, Power Electronics and Drives (SDEMPED), Valencia, Spain, August 2013, pp. 520–526
[23] Gritli, Y., Tani, A., Rossi, C., *et al.*: 'Experimental assessment of winding inter-turn short-circuits in six-phase AC permanent magnet synchronous motors'. 2019 Int. Conf. on Clean Electrical Power (ICCEP), Otranto, Italy, July 2019, pp. 29–35
[24] Bianchi, N., Bolognani, S., Pre, M.D.P.: 'Impact of stator winding of a five-phase permanent-magnet motor on Postfault operations', *IEEE Trans. Ind. Electron.*, 2008, **55**, (5), pp. 1978–1987
[25] Gritli, Y., Tani, A., Rossi, C., *et al.*: 'Detection of rotor magnet demagnetization in asymmetrical six-phase surface mounted permanent magnet synchronous motor drive'. Proc. - 2018 23rd Int. Conf. Electrical Machines ICEM, Alexandroupoli, Greece, September 2018, pp. 1809–1814
[26] Grandi, G., Serra, G., Tani, A.: 'General analysis of multi-phase systems based on space vector approach'. 2006 12th Int. Power Electronics and Motion Control Conf., Portoroz, Slovenia, Aug.–Sept. 2006, pp. 834–840
[27] Gritli, Y., Casadei, D., Tani, A., *et al.*: 'Validation of rotor magnets demagnetization detection in six-phase surface-mounted AC permanent magnet synchronous motors'. SPEEDAM 2018 - Proc.: Int. Symp. on Power Electronics, Electrical Drives, Automation and Motion, Amalfi, Italy, June 2018, pp. 224–229